Correlation between Coke Type, Microstructure and Anodic Reaction Overpotential in Aluminium Electrolysis

Rebecca Jayne Thorne[1*], Camilla Sommerseth[1], Arne Petter Ratvik[2], Stein Rørvik[2], Espen Sandnes[3], Lorentz Petter Lossius[3], Hogne Linga[3], and Ann Mari Svensson[1]

[1]Dept. of Materials Science and Engineering, Norwegian University of Science and Technology, NO-7491 Trondheim, Norway

[2]SINTEF Materials and Chemistry, NO-7465 Trondheim, Norway

[3]Norsk Hydro ASA, NO-6881 Årdalstangen, Norway

[*]Corresponding author. Tel: +47 400 85886. Email: rjt@nilu.no. Present address: Department of Environmental Impacts and Economics (IMPEC), Norwegian Institute for Air Research (NILU), PO Box 100, NO-2027 Kjeller, Norway

Keywords: Carbon anode, aluminium electrolysis, isotropy, electrochemical reactivity, microstructure

Abstract

Although the anode process during aluminium electrolysis has a substantial overpotential that increases the energy demand and production cost of aluminium, properties of the coke that can influence the electrochemical reactivity in the industrial anode itself have not been well documented. In this work the electrochemical performance of anodes fabricated from single source (anisotropic and

isotropic) cokes, including an ultrapure graphite as reference material, was determined, and compared to the material properties of the cokes and baked anodes. Cokes and anodes were characterised with respect to air and CO_2 reactivity, optical texture, presence of oxygen surface groups, as well as to microstructure (fractions of basal, edge and defect sites on the surface and pore volume below 16 nm). Results show that anodes made from more isotropic cokes (increasing optical texture fineness) had a slight improvement in the electrochemical performance compared to those made from more anisotropic cokes. For all anodes, electrochemical reactivity correlated well with the electrochemically-wetted surface area, as determined by the double layer capacitance. This appears to be related to microstructure and the volume of pores with width below 16 nm, and possibly also to differences in surface chemistry, rather than differences in surface roughness and porosity as determined by optical techniques (i.e. on a μm-scale).

1. Introduction

Efforts to lower energy consumption continue to be one of the major challenges of aluminium production [1, 2]. At the anode the overpotential can be as high as 0.6 V, representing one major area where energy can be saved within the aluminium production process.

In an aluminium reduction cell, oxide ions from the dissolution of alumina in cryolite are discharged electrolytically to form CO_2 on the carbon anode, whilst aluminium metal is formed on the cathode. A prebaked carbon anode is made from a fractioned, sized and re-blended petroleum coke aggregate, which is mixed with around 12-15

wt% coal tar pitch binder and baked at approximately 1200 °C. The total time for baking (loading in the baking furnace, heating to temperature, holding time, cooling and unloading anodes) may take 10-12 days. Equations 1a, b and c show the electrode half reactions at the anode, cathode, and the overall reaction equation respectively, where E^0_{CO2} = 1.187 V vs Al/Al^{3+} [3]. The anode reaction is thought to proceed via two electrochemical steps with an intermediate compound adsorbed on the electrode [4, 5]. An example scheme for the reaction is shown in Equations 2a and b [4], although the specific oxyfluoride species involved are disputed [6, 7].

$$6O^{2-} + 3C \rightarrow 3CO_2 + 12e^- \qquad (1a)$$

$$4Al^{3+} + 12e^- \rightarrow 4Al \qquad (1b)$$

$$2Al_2O_{3(diss)} + 3C_{(s)} \rightarrow 4Al_{(l)} + 3CO_{2(g)} \qquad (1c)$$

$$Al_2O_2F_6^{4-} + C \rightarrow CO_{ads} + Al_2OF_6^{2-} + 2e^- \qquad (2a)$$

$$Al_2O_2F_6^{4-} + CO_{ads} \rightarrow CO_2 + Al_2OF_6^{2-} + 2e^- \qquad (2b)$$

The un-compensated potential of the anode in an aluminium reduction cell, measured versus a reference electrode ($E_{anode,\ measured}$), is given in Equation 3.

$$E_{anode,\ measured} = E^{rev} + \eta_c + \eta'_r + \eta_h + I\cdot(R'_s + \delta R_s) \qquad (3)$$

As concentration overpotential (η_c) at the anode in this system may be considered as negligible [8], the anode overpotential approximates to the reaction overpotential (η'_r). This is a specific charge transfer overpotential term developed to relate to electrode reactions where intermediate adsorption/desorption plays a decisive role. In addition,

gas produced at the anode has two dominating effects; an increase in ohmic resistance, mainly caused by the reduced effective anode surface area, and an increase in overpotential due to higher current density at the reduced surface. The first term (δR_s) denotes the increase in the ohmic resistance due to partial blocking of the surface with bubbles, and R'_s equals the ohmic resistance with no bubbles screening the surface. The second part is observed as an increase in the reaction overpotential. The additional overpotential due to the reduced effective surface area caused by bubble screening is commonly denoted hyperpolarisation, η_h [9, 10]. In a similar representation as above, $\eta_r = \eta'_r + \eta_h$, where η'_r equals the reaction overpotential with no bubble screening of the anode surface. Other terms in Equation 3 include E^{rev}, the reversible potential for the CO_2 forming reaction, and I, the current.

At the nanoscale, it has been shown that the electrochemically or oxidatively reactive sites on the surface of graphitic carbon materials are not homogeneously distributed, but that edge sites have a higher chemical and electrochemical reactivity than the basal planes [11, 12]. For anode materials, it is considered well established that graphite gives a higher overpotential than baked carbon [3]. For example, Dewing and van der Kouwe [13] found that the overpotential of baked carbon electrodes (Søderberg type) was 100 mV less than grade ATJ graphite. Similarly, the results of Jarek and Orman [14] indicate a difference of approximately 80 mV between the overpotential of a graphite anode and a baked anode at around 1 A cm^{-2}.

It needs to be kept in mind, however, that the electrochemical reactivity of anodes is also influenced by surface roughness and impurities, as well as wetted surface area; parameters that will also vary with choice of coke and fabrication procedures. Jarek

and Thonstad [15], for example, showed how the scatter in polarisation curves was reduced when differences in wetted area of anodes subject to different baking temperatures were accounted for. Djokic et al. [16] electrochemically characterised both graphite electrodes and a glassy carbon electrode, and found that the reaction mechanism of the anodic process depended on the nature of the carbon electrode. For glassy carbon, the cyclic voltammograms indicated a diffusion controlled process, by O^{2-} or oxyfluoride anions. For graphite, a complex mixed activation and diffusion controlled process was proposed, involving adsorption and/or reaction of the oxygen containing electroactive species at the electrode surface.

The majority of laboratory studies relating anode properties to electrochemical reactivity have focused on the effects of anode impurities, mostly simulated by chemical doping. Generally, it is observed that metals such as iron, vanadium, calcium and sodium can lower the overpotential. Negative effects relating to the presence of anode electrocatalyst impurities include the acceleration of the excess reaction of carbon with air and CO_2 [17-19]; impurities may also dissolve in the electrolyte adding to the current efficiency loss [20] and eventually, all metal impurities in the anode will end up in aluminium, thus lowering the purity [3]. A good overview of the effects of impurities on overpotential has been given by Thonstad [3]. For example, by using an Fe_2O_3 additive to raise iron concentrations in anodes from 450 ppm to 4280 ppm (0.42 %), Haarberg et al. [21] observed lowered overpotential by 100 mV. Thonstad and Hove [22] observed smaller changes in overpotential; up to 7 mV when they doped anodes with 1.3 wt% Fe_2O_3 or 0.6 wt% Na_2CO_3. However, artificially added dopants cause un-realistically high impurity

levels and are not fully incorporated into the coke bulk structure. Thus, artificially doped cokes are not fully representative of real cokes.

Most previous electrochemical studies of anodes are based on glassy carbon, graphite, or generic (not well characterised) industrial anodes. In general, few details about the history and production of the carbon anode are given and it is difficult to draw any conclusions regarding the role of the carbon material. Within industry, routinely measured anode parameters include air and CO_2 reactivity, specific electrical resistivity (SER), density, permeability and various mechanical properties, but no reported test directly measures electrochemical reactivity routinely. The aim of this work was therefore to determine the electrochemical reactivity of anodes made from single source cokes, and relate it to the anode chemical/physical properties including isotropy, microstructure and impurity levels. Here, isotropy is defined in terms of the optical domains which form during the semi-liquid mesophase stage preceding carbonisation, where the size of domains is determined by how far the melting together, or coalescence, of mesophase droplets progresses. A vertical anode was designed and used, in order to measure the electrochemical reactivity with a minimum contribution from bubbles. Understanding these relationships is particularly important in light of the fact that the coke quality available for anode production is changing [23-25]; with anode grade coke increasing not only in certain impurity concentrations, but also in isotropy.

2. Materials and Methods

Pilot scale anodes were produced by Norsk Hydro ASA from five single source cokes (particle size 0-2 mm) varying in isotropy, as described previously [26-28]. Aside from coke type, all other production parameters were kept constant. Anodes 1-4 were made from petroleum cokes and Anode 5 from a coal tar pitch based coke. A graphite material (Ultrapure grade CMG, provided by Svensk specialgrafit AB) was also used for comparison in the anode series.

2.1. Optical texture and surface structure characterisation

Anodes were characterised for density, air and CO_2 reactivity and SER (according to ISO 12985-1:2000 and Norsk Hydro ASA in house methods similar to ISO 12989-1:2000, ISO 12988-1:2000 and ISO 11713:2000), where the ISO-X numbers are international standards developed by the International Organisation for Standardisation (ISO). Anode impurities (metal and sulphur content) were characterised using an X-ray fluorescence method according to ISO 12980:2000.

To characterise optical texture, epoxy-mounted and polished (to 1 µm) samples were studied under polarised light using optical microscopy (high-end Leica/Relchert MeF3A metallurgical optical reflecting light microscope). Compound images were produced of 192 individual frames, taken by scanning across the surface at a magnification of x250. Analysis software, as developed by Rørvik et al. [29], was subsequently used on the individual images to quantify isotropy in terms of mosaic and fibre index, parameters relating to the degree of isotropy and anisotropy respectively. Isotropic materials are defined as having a high mosaic index, a parameter that describes the fineness of the optical domains, whereas anisotropic materials have a high fibre index, a parameter that describes the alignment of optical

domains. A rolling average for each parameter was taken over the individual 192 image frames for each anode to study structural homogeneity, and two parallels were performed for each anode material using different samples.

Surface oxides attached to edge sites were quantified by a temperature ramping program using LECO oxygen analysis (LECO analyser model TC-436DR). Analysis were performed on fines produced from all five cokes, their corresponding anodes and ultrapure graphite (particle size <63 µm). As different oxide species react with carbon to form CO and CO_2 at different temperatures, surface oxides could be distinguished from impurity-related oxide peaks by a comparison with the ultrapure graphite. Samples (~0.1 g) were packed into tin capsules (from LECO corp.), and sample oxygen was reacted by ramping power between 0-5000 W at 20 W s^{-1} whilst measuring CO and CO_2 off-gases. Power was converted to the temperature equivalent (°C) using a calibration curve.

Nitrogen adsorption measurements were performed at -198.5 °C in full range of the relative pressure using a Tristar II 2030 apparatus (Micrometrics). Analysis was again performed on fines produced from all five cokes, their corresponding anodes and ultrapure graphite (particle size <63 µm). Before analysis, samples (~0.5 g) were degassed for 12 hours at 300 °C. Measurement of the specific surface area of the materials was performed on the basis of the Brunauer-Emmett-Teller (BET) theory and equation, using the standard instrument software. The contributions of edge:basal:defect sites were determined from the nitrogen adsorption data using a density functional theory (DFT) based model developed by Olivier et al. [30, 31], which accounts for surface heterogeneity by introducing variations in adsorptive

potential for the basal, edge and defect sites. The model is implemented in the software of the Tristar II 2030 apparatus (DFT Plus package). Based on previous work, the adsorptive potentials, expressed in Kelvin, for graphitic materials are in the range 20 – 49 K for edge planes, 50 – 60 K for basal planes and 61 – 100 K for defects [30, 32]. An example of application and verification of the theory for graphitic powder can be found in [30] Adsorption energies were found to change with sample age, so all work was carried out on freshly made particle fines. Three or two sample parallels were performed for LECO and nitrogen adsorption measurements, respectively.

2.2. Electrochemical testing

Anodes were cut and assembled as schematically depicted in Figure 1a. Components were threaded together on a 3 mm diameter graphite rod that was attached via a graphite connector to a stainless steel contact bar. Advantages of the vertical design were a defined anode area for melt immersion (1.57 cm^2), an even current distribution and a minimised bubble retention during electrolysis. To verify that bubbles were not being retained on the surface, the vertical anodes were compared against anodes with horizontal faces and a graphite rod, as described in [28] and [26], respectively. A schematic of the electrochemical setup is shown in Figure 1b, which was contained within a tube furnace at 1000 °C in an argon atmosphere. The three electrode system compromised of the anode material as working electrode, graphite crucible as counter electrode, and an aluminium reference electrode as described in [33].

Electrochemical testing was performed in a cryolite melt with a molar ratio of sodium fluoride to aluminium fluoride of 2.3 (Sigma Aldrich >97 %) corresponding to 9.8

wt% excess AlF_3 (industrial grade, sublimed in-house) and 9.4 wt% γ alumina (Merck). Measurements were made using a Zahner IM6 with built in Electrochemical Impedance Spectroscopy (EIS) module and 20 A booster (PP201, from Zahner-Elektrik). EIS was used to determine the ohmic resistance at the Open Circuit Potential (OCP), the value of which was used to IR compensate all electrochemical measurements. The potential of the anodes (with respect to Al reference) was measured at a current density of 1 A cm^{-2}, close to the anode current density in modern industrial cells. EIS was additionally performed at 1.4 V, and the polarisation resistance (R_{pol}) extracted from Nyquist plots by subtracting the high frequency Z' intercept from the low frequency Z' intercept. After subtracting the points relating to the low frequency inductive loop, data was fitted to a LR(CR) equivalent circuit in order to extract anode capacitance. Three consecutive scans of cyclic voltammetry (CV) between OCP and 2.5 V at 0.1 V s^{-1} were performed, as previous experiments showed that sweep-rates up to 0.1 V s^{-1} gave similar results to steady-state polarisation curves. Four anode parallels (using fresh anodes) were performed and the order of the anode materials tested was randomised to eliminate possible changes in the melt and reference electrode over time.

3. Results and discussion

3.1. Optical texture and surface structure characterisation

Selected anode properties are listed in Table 1. Anodes were similar in terms of density and SER, but those made from the most isotropic cokes (Anodes 3 and 4) had highest air reactivity. Anode 5, made from a pitch based coke, had lowest air reactivity amongst the pilot anodes, but the highest CO_2 reactivity in the series.

Generally, air reactivity correlated positively with metal impurities, possibly due to catalytic effects [17-19]. The exception was Anode 5, made from a pitch-based rather than petroleum-based coke. For the industrial coke-based anodes, sulphur seemed to generally correlate negatively with CO_2 reactivity, as observed also by others [34].

Viewed using optical microscopy under polarised light, a trend of increasing isotropy was observed from graphite and Anodes 1 and 2, to Anodes 3 and 4, as shown by anode grain fineness and orientation. Anode 5 was lower in isotropy. Figure 2 shows single image frames of the anodes taken at x250 magnification under polarised light, and software developed to analyse the optical texture of the images [29] confirmed visual isotropy trends. Due to the fact that the mosaic and fibre index, parameters described in [29] relating to the fineness and the alignment of optical domains respectively, were relatively constant with number of frames, the final 'average' values of the 192 frames could be taken as representative of each material. These are shown in Figure 3. Within the anode series, the mosaic index was higher for Anodes 3-5 than graphite and Anodes 1-2, and the fibre index was higher for Anodes 1-2 and lower for Anodes 3-5. For most samples, a high mosaic index value correlated as expected with a low fibre index value. The graphite actually had a more isotropic optical texture in terms of mosaic and fibre index than Anodes 1 and 2 due to its production from milled calcined coke, with optical texture not due to mesophase coalescence as for the other materials. As expected, the chemical (air) reactivity of the carbon anode materials decreased with increasing structural ordering (*cf.* Table 1).

The nanoscale surface coverage of edge, basal and defect sites particles of Cokes 2-5 and all the anodes was determined using nitrogen adsorption, following the work of

Olivier et al [30-32]. A typical plot for the distribution of incremental surface area measured *vs.* energy of the samples is shown in Figure 4, and summed surface coverage of edge sites, basal planes and defect sites on cokes and their respective anodes are shown in Figure 5. The surface of all the coke and crushed anode particles were dominated by edge sites, with high fractions of defect sites, but only low fractions of basal planes. The low fraction of basal planes disappeared entirely for the crushed anodes, possibly due to remnants of pitch covering the coke particles. The coverage of defect sites decreased with coke and anode isotropy, whilst the coverage of edge sites increased with isotropy. It is reasonable to assume that the results are applicable also to the coke fractions actually used for the fabrication of the anodes. The corresponding volumes of pores (width <16 nm), as determined from the BET analysis, are shown in Figure 6 for Cokes 1-5. These are relatively low, showing the coke particles to have few pores with a width below 16 nm, although previous work shows the anodes contain many larger pores on µm scale (~10-200 µm diameter) [28]. Representative isotherms have been included for all materials in supplementary information (S1 and S2); these resemble those classified as type II isotherms [35], which are observed for macroporous or nonporous carbons, representing monolayer-multilayer adsorption. For some materials (graphite, Cokes 3 and 5 and Anodes 3 and 5), a hysteresis resembling type H3 (B) hysteresis is indicative of slit shaped pores [35], although the hysteresis is generally small.

The amount of oxygen present in the samples was measured by LECO, providing information on surface oxygen groups [12], and the presence of metal oxides. In graphite, there was only one major peak exhibited on both CO and CO_2 off-gas curves with increasing temperature. As this graphite was ultrapure, the peak was attributed

to the combustion of surface oxygen with carbon. Figures 7 and 8 show CO and CO_2 curves for all materials. A broad additional peak of CO/CO_2 given off at higher temperatures indicated the presence of other oxides – probably complexed with metals. This was particularly pronounced for the more isotropic materials.

Differences in evolved CO and CO_2 can in principle be related to the various oxygen surface groups. Figueiredo et al. [36] provide a good review of carbon surface group decomposition products and expected reaction temperature, suggesting that CO_2 is produced from the decomposition of carboxylic, lactone and anhydride groups, whilst CO is produced from phenol, carbonyl, anhydride, ether and quinone groups. The LECO analysis is expected to be very accurate with respect to quantification of amount of CO and CO_2 released, but due to the rapid heating (approximately 1000 °C min^{-1} compared to ~5 °C min^{-1} for temperature programmed desorption), peak temperatures, and hence individual oxygen surface groups, could not be identified for the materials in this study. Nevertheless, due to the presence of two CO_2 peaks in the lower temperature range of the more isotropic cokes and anodes, compared to one peak in the more anisotropic materials, a wider range of surface groups may be present on more isotropic materials. Also, due to the lower CO:CO_2 ratio, the surface of isotropic cokes may be assumed to be richer in acidic oxygen surface groups, as these will primarily desorb as CO_2 [37]. The higher ratio of CO_2 for the more isotropic cokes correlates well with their high air reactivity as shown in Table 1. As with the nitrogen adsorption results, measured variation in surface structure amongst the anode particles may be less due to remnants of pitch covering the coke surface. Future work should investigate further the different surface species present using, for example, Fourier transform infrared spectroscopy (FTIR).

Through the separate integration of both CO and CO_2 curves, sample oxygen relating to either the edge site (surface) oxygen peak at low temperatures (seen in graphite), or relating to the metal oxide peak at higher temperatures, was calculated; see Figure 9 for integration details. For CO curves, the tail end of the edge site peak seen in graphite was also accounted for (Figure 9a), probably related to strong binding and hence slow reaction kinetics. Figure 10 shows the resulting total metal oxide and surface oxide concentrations (the latter normalised for BET surface area).

The more isotropic materials had a large amount of metal oxides present, as expected from the known metal impurity values shown in Table 1; metals such as vanadium are generally assumed to exist in cokes and anodes as oxides such as V_2O_3 [38]. Interestingly, the concentration of metal oxide oxygen was of the same order of magnitude as the metal impurities. For example, Anode 4 contained 2430 ppm metals and 0.1640 wt% (1640 ppm) metal oxide oxygen. As it is therefore likely that most oxygen is complexed with metals, this suggests that the high levels of sulphur present in some of the anodes (4.45 % in Anode 4) may predominantly exist in an un-oxidised form.

3.2 Electrochemical testing

To measure η_r with a minimum contribution from bubbles, an anode with only vertical immersed active area was designed and used. The potential of the graphite vertical anode *vs.* time was compared against a graphite anode with only horizontal active surface area, and a graphite rod with both horizontal and vertical surfaces (Figure 11).

Where horizontal surfaces were present on the anode, the potential oscillated in a saw-tooth curve. This can be explained by the fact that as bubbles formed, the potential increased due to a combination of increased series resistance mainly due to anode screening and hyperpolarisation due to a reduction in effective anode surface area [10, 39]. When bubbles were released, the potential dropped sharply due to an immediate decrease of series resistance and increase in effective surface area, minimising hyperpolarisation. In contrast, when the vertical anode was used, only very small oscillations were observed. These small oscillations possibly resulted from the evolution of very small bubbles from the surface; to be expected even on vertical anodes as studies have shown that the surface of a stationary vertical anode can be covered by 20 % gas bubbles at any one time [9, 10]. In another study using rotating vertical anodes with a diameter of 1.27 cm^2, the hyperpolarisation caused by bubbles screening the anode surface was 8 mV at 1 A cm^{-2} [8, 9]. In contrast, in industrial situations using anodes with large horizontal surfaces, studies have estimated an extra ohmic voltage drop in the range of 0.15-0.35 V due to bubble screening [40]. All following results were therefore obtained with the vertical geometry in Figure 1a.

Potentials of the anode materials in the series at 1 A cm^{-2} (w.r.t Al reference) are shown in Figure 12a, and quoted with respect to graphite in Figure 12b. As η_c is considered negligible in saturated melts, differences in measured potential between the anodes relate approximately to differences in reaction overpotential, η'_r. Measured overpotential and polarisation resistance are quoted with respect to graphite electrodes measured in the same sequence in order to minimise the scatter in the results typically observed in these high temperature systems. Results showed that at 1 A cm^{-2}, η'_r of the anodes made from the single source cokes was in the range 100-170 mV lower

than the overpotential of the graphite, with a very slight decrease in overpotential throughout the series, as additionally found in the preliminary study [29]. Differences between graphite and coke-based anodes are also similar to the findings of Dewing and van der Kouwe [13], and Jarek and Orman [14]. Maximum variation in the potential at 1 A cm^{-2} of the industrial coke-based anodes was ~60 mV. Although lower than the variation measured previously [29], averages were generally within the high error of the preliminary study, highlighting the difficulties of working with inhomogeneous materials coupled with a small anode area.

Figure 12 also includes the differences in overpotential at 1 A cm^{-2} obtained from CV scans at 0.1 V s^{-1}, which may be assumed to be very close to steady state experiments. Examples of these curves are shown in Figure 13 for Anodes 1 and 5, as well as the graphite. As seen from Figure 12, all coke-based anodes show small currents below E^0_{CO2} (1.187 V [3]) but above E^0_{CO} (1.065 V [3]), which may be attributed to a CO-forming reaction at low current densities (below 0.1 A cm^{-2}), as reported also by others [41]. As the graphite anode has a very smooth and dense surface compared to the coke anodes, direct comparison of the electrochemical performance has not been emphasised in this study. A previous study using the same anode materials found no significant differences in the gaseous reaction products between Anodes 2-4 [26]. Nonetheless, at typical operating conditions of 1 A cm^{-2}, the CO_2 reaction is the dominating one. The electrochemical reactivity of the anodes appeared to correlate somewhat with the air reactivity, except for the pitch coke anode. This may be related to differences in the type of impurities present, but further investigation of this is beyond the scope of this study.

Nyquist plots obtained for all anodes at 1.4 V are shown in Figure 14. Data is not fitted, but lines are drawn between measurement points for clarity. As can be seen, the spectra exhibited a low frequency inductive loop (negative values of –Z''), characteristic of electrochemical processes involving an intermediate adsorption step, as shown by Harrington and Conway [42]. The polarisation resistance was extracted from unfitted Nyquist plots by subtracting the high frequency Z' intercept from the low frequency Z' intercept. Figure 15a shows how R_{pol} changed with anode type. For graphite and Anodes 1-5, average R_{pol} values were 0.47 Ω, 0.16 Ω, 0.16 Ω, 0.13 Ω, 0.13 Ω and 0.14 Ω respectively. Thus, R_{pol} correlated with η'_r, showing small changes amongst the industrial coke-based anodes. The polarisation resistance of the graphite was not directly comparable to the coke-based anodes at 1.4 V due to the higher onset potential of the graphite, but the polarisation resistance of 0.26 Ω obtained from the impedance spectrum on graphite at 1.6 V reflects the differences in reactivity.

After removal of data relating to the low frequency inductive loop, a LR(CR) model was used to extract anode capacitance. The low frequency inductive loops are typically related to intermediate adsorption processes [43]. The double layer capacitance is generally regarded as the best method for assessment of the wetted surface area during polarisation [15]. The average capacitance values for graphite in this study (23 μF cm^{-2} at 1.4 V and 32 μF cm^{-2} at 1.6 V) are similar to values recorded by Jarek and Thonstad [15], attributed to the anode double-layer capacitance for non-porous graphites. As shown in Figure 15b, anode capacitance at 1.4 V increased substantially from graphite through Anodes 1 and 2 (121 μF cm^{-2} and 117 μF cm^{-2}) to Anode 3 (175 μF cm^{-2}), and decreased slightly to Anodes 4 and 5 (140 μF cm^{-2} and 131 μF cm^{-2}). This does not seem to correlate with the real area of the anodes, studied

previously using confocal microscopy [28], and may instead relate to the wettability of the anodes with electrolyte. Previous results showed that Anodes 3-5 had higher wettability with the electrolyte than Anodes 1-2 and graphite [28]. Although these electrolyte wetting measurements were performed on the anodes when unpolarised, and do not correlate perfectly with capacitance, wetting is still a plausible contribution to the observed capacitance variation at 1.4 V.

The differences in the wetted surface area, as determined by the double layer capacitance, are not likely to be fully related to the surface structure, as all cokes appear to have a high fraction of edge sites. It seems also not related to surface roughness as determined by optical techniques (i.e. on the μm) scale. From the cross-sections of the cylindrical samples, all the coke anodes had a surface roughness ratio between 1.2 and 1.4 [28]. The industrial coke-based anodes also have a very similar total porosity (10-12 %) of pores in the μm range [28]. Similar findings were also presented in [15], where no correlation between C_{dl} and the volume of anode pores in the range 0.01 to 70 μm was observed. It is interesting to notice that the more isotropic cokes, which are also the ones with the best wetting properties, have a higher ratio of CO_2:CO as measured by LECO. Typically, oxygen surface groups that are released as CO_2 are generally associated with acidic properties of the carbon surface. As seen from Figure 6, the isotropic Cokes (3, 4 and 5) have a higher volume of pores (width < 16 nm) compared to the anisotropic cokes (1 and 2). Coke 5 has the highest cumulative pore volume in this range, but also the lowest ratio of CO_2:CO.

Generally, anodes with highest electrochemical reactivity had highest air reactivity; an increase in air reactivity has been linked to a small increase in electrochemical

reactivity in some [22] but not all studies. Electrocatalytic effects resulting from metal impurities may go some way to explaining results, due to the correlation of coke isotropy and anode metal impurity content. In contrast, the specific effect of sulphur on overpotential in this study is likely to be minimal, due to the very low sulphur levels in Anode 5 compared to Anode 4 but a similar overpotential of each. Needless to say, the naturally occurring range of total metal impurity concentrations of the anodes here is smaller than those used in many doping studies [21, 22], making it unlikely that metal impurities explain all the trends observed in this study.

Potential differences between the coke-based anodes in this study were much smaller than differences in another study where the same materials were electrolysed in a horizontal design [28]. In this geometry, the mid-point potential of the coke-based anodes varied by up to 200 mV. This suggests that the materials are much more different in terms of their CO_2/electrolyte/carbon wettability and bubble evolution properties (η_h and δR_s) than η'_r. Nevertheless, studying individual parameters and anode properties separately is important in order to resolve and explain anode reactivity differences at a fundamental level, although this is difficult to perform in natural coke and anode situations due to the correlation of many properties, and often small variation between materials.

4. Conclusions

The focus of this work was to compare various anodes made from single-source cokes and a graphite anode with respect to electrochemical reactivity, and correlate with chemical/physical parameters. The more isotropic cokes had higher levels of

impurities compared to the more anisotropic cokes, and appeared to have a slightly higher fraction of edge sites and different oxygen surface groups, as reflected by the higher ratio of CO_2:CO evolved during LECO experiments. Anodes made from these isotropic cokes had on average a slightly lower anodic overpotential, which also correlated with the electrochemically active surface area as determined by the double layer capacitance. The differences may be related to a small variation in fraction of edge sites and/or pores with width < 16 nm among the anodes, differences in the oxygen surface groups, or possibly also metal impurity concentrations.

Acknowledgements

This work was financed by Norsk Hydro ASA and the Research Council of Norway, grant number 210899/030**.** Thanks are due for the great work performed by Aksel Alstad at the NTNU workshop where fabrication of experimental parts was required, and to Anne Støre, Ole Kjos and Egil Skybakmoen at SINTEF for their helpful contributions. Additionally, Kirsti Gulbrandsen and other laboratory employees within Norsk Hydro ASA are acknowledged for the XRF analysis, density, SER and reactivity measurements.

References

1. T.E. Norgate, S. Jahanshahi and W.J. Rankin: J. Cleaner Prod., 2007, 15(8–9), pp. 838-48.
2. H. Kvande and W. Haupin: JOM, 2000, 52(2), pp. 31-7.
3. J. Thonstad, P. Fellner, G.M. Haarberg, J. Hives, H. Kvande and Å. Sterten: Aluminium Electrolysis: Fundamentals of the Hall-Héroult process, 3rd ed., Aluminium-Verlag Marketing & Kommunikation GmbH, Breuerdruck, Germany, 2001, pp. 159, 181-3.
4. A. Kisza, J. Thonstad and T. Eidet: J. Electrochem. Soc., 1996, 143(6), pp. 1840-7.
5. G. Picard, E. Prat, Y. Bertaud and M. Leroy: In R. D. Zabreznik (editor): Light Metals 1987, The Minerals, Metals & Materials Society (TMS), Warrendale, PA, 1987, pp. 507-17.
6. J. Thonstad, A. Kisza and J. Kazmierczak: J. Appl. Electrochem., 1996, 26(1), pp. 102-12.
7. Å. Sterten: Electrochim. Acta., 1980, 25(12), pp. 1673-7.
8. J.A. Leistra and P.J. Sides: In R.B. Miller and W.S. Peterson (editors): Light Metals 1986, The Minerals, Metals & Materials Society (TMS), Warrendale, PA, 1986, pp. 473-8.
9. J.A. Leistra and P.J. Sides: J. Electrochem. Soc., 1986, 133(3), pp. C119-20.
10. J.A. Leistra and P.J. Sides: Electrochim. Acta., 1988, 33(12), pp. 1761-6.
11. C.E. Banks, T.J. Davies, G.G. Wildgoose and R.G. Compton: Chem. Commun., 2005, (7), pp. 829-41.
12. N.R. Laine, F.J. Vastola and P.L. Walker: J. Phys. Chem., 1963, 67(10), pp. 2030-4.
13. E.W. Dewing and E.T. Vanderkouwe: J. Electrochem. Soc., 1975, 122(3), pp. 358-63.
14. S. Jarek and Z. Orman: Electrochim. Acta., 1985, 30(3), pp. 341-5.
15. S. Jarek and J. Thonstad: J. Appl. Electrochem., 1987, 17(6), pp. 1203-12.
16. S.S. Djokic, B.E. Conway and T.F. Belliveau: J. Appl. Electrochem., 1994, 24(9), pp. 827-34.
17. Z. Kuang, J. Thonstad and M. Sørlie: Carbon, 1995, 33(10), pp.1479-84.

18. J. Rolle and Y. Hoang: In J.D. Evans (editor): Light Metals 1995, The Minerals, Metals & Materials Society (TMS), Warrendale, PA, 1995, pp. 741-5.
19. M. Sørlie and T. Eidet: In B. Welch (editor): Light Metals 1998, The Minerals, Metals & Materials Society (TMS), Warrendale, PA, 1998, pp. 763-8.
20. W. Haupin: J. Electrochem. Soc., 1973, 120(1), pp. 83-5.
21. G.M. Haarberg, L. Solli and Å. Sterten: Proc. 7th Slovak Aluminium Symp., Banska Bystrica, Slovakia, 1993, pp. 95-101.
22. J. Thonstad and E. Hove: Can. J. Chem., 1964, 42(7), pp. 1542.
23. L. Edwards, N. Backhouse, H. Darmstadt and M.J. Dion: In C.E. Suarez (editor): Light Metals 2012, The Minerals, Metals & Materials Society (TMS), Warrendale, PA, 2012, pp. 1207-12.
24. L. Edwards, F. Vogt, M. Robinette, R. Love, A. Ross, M. McClung, R.J.Roush and W. Morgan: In G. Bearne (editor): Light Metals 2009, The Minerals, Metals & Materials Society (TMS), Warrendale, PA, 2009, pp. 985-90.
25. F. Vogt, R. Tonti, M. Hunt and L. Edwards: In A.T. Tabereaux (editor): Light Metals 2004, The Minerals, Metals & Materials Society (TMS), Warrendale, PA, 2004, pp. 489-93.
26. R.J. Thorne, C. Sommerseth, E. Sandnes, O.S. Kjos, T.A. Aarhaug, L.P. Lossius, H. Linga and A.P. Ratvik: In B. Sadler (editor): Light Metals 2013, The Minerals, Metals & Materials Society (TMS), Warrendale, PA, 2013, pp. 1207-11.
27. R. J. Thorne, C. Sommerseth, A.M. Svensson, E. Sandnes, L.P. Lossius, H. Linga and A.P Ratvik: In J. Grandfield (editor): Light Metals 2014, The Minerals, Metals & Materials Society (TMS), Warrendale, PA, 2014, pp. 1213-7.
28. R.J. Thorne, C. Sommerseth, A.P. Ratvik, S. Rørvik, E. Sandnes, L.P. Lossius, H. Linga and A.M. Svensson: JES, 2015, 162(8), pp. E104-14
29. S. Rørvik, M. Aanvik, M. Sorlie and H.A. Øye: In R.D. Peterson (editor): Light Metals 2000, The Minerals, Metals & Materials Society (TMS), Warrendale, PA, 2000, pp. 549-54.
30. J.P. Olivier and M. Winter: J. Power Sources, 2001, 97-8, pp. 151-5.

31. J.P. Olivier: In E.J. Bottani and J.M.D. Tascón (editors): Adsorption by carbons 2008, Elsevier, Oxford, 2008, pp. 147-66.
32. N.D. Connell and E.R. Baker (editors): Surfaces of nanoparticles and porous materials, CRC Press, Florida, 1999.
33. O.S. Kjos, T.A. Aarhaug, H. Gudbrandsen, Å. Solheim and E. Skybakmoen: In B. Welch, G. Stephens, J. Metson and M. Skyllas-Kazacos (editors): Proc. 10th AASTC: University of New South Wales, Launceston, Tasmania, 2011, pp. 4b1.
34. S. Pietrzyk and J. Thonstad: In C.E. Suarez (editor): Light Metals 2012, The Minerals, Metals & Materials Society (TMS), Warrendale, PA, 2012, pp. 659-64.
35. A. Linares-Solano: In J.L. Figueiredo and J.A. Moulijn (editors): Carbon and coal gasification: Science and technology, Springer Science & Business Media: Dordrecht, 2012, p. 142-5.
36. J.L. Figueiredo, M.F.R. Pereira, M.M.A. Freitas and J.J.M. Orfao: Carbon, 1999, 37(9), pp. 1379-89.
37. H. Marsh, E.A. Heintz, and F. Rodriguez-Reinoso (editors): Introduction to carbon technologies, University of Alicante, 1997.
38. K.N. Tran, A.J. Berkovich, A. Tomsett and S.K. Bhatia: Energy Fuels, 2009, 23, pp. 1909-24.
39. J.L. Xue and H.A. Øye: In J.W. Evans (editor): Light Metals 1995, The Minerals, Metals & Materials Society (TMS), Warrendale, PA, 1995, pp. 265-71.
40. W. Haupin: JOM, 1971, 23(10), pp. 46.
41. S. Jarek and J. Thonstad: J. Electrochem. Soc., 1987, 134(4), pp. 856-9.
42. D.A. Harrington and B.E. Conway, Electrochim. Acta., 1987. 32(12), pp. 1703-12.
43. A. Kisza: Electrochim. Acta., 2006, 51(11), pp. 2315-21.

Table 1

Anode	[Metals] / ppm	[S] / %	Reactivity / mg cm^{-2} h^{-1}		SER / μΩ m	Density / g cm^{-3}
			Air	CO_2		
Graphite	66	0.00	0.3	2.5	12.7	1.771
Anode 1	683	0.94	39.0	19.0	55.2	1.603
Anode 2	932	2.40	29.5	5.9	52.0	1.627
Anode 3	1976	4.18	69.6	7.2	47.2	1.614
Anode 4	2430	4.45	70.1	7.4	50.5	1.596
Anode 5	2413	0.37	17.7	26.7	42.3	1.648

Figure 1

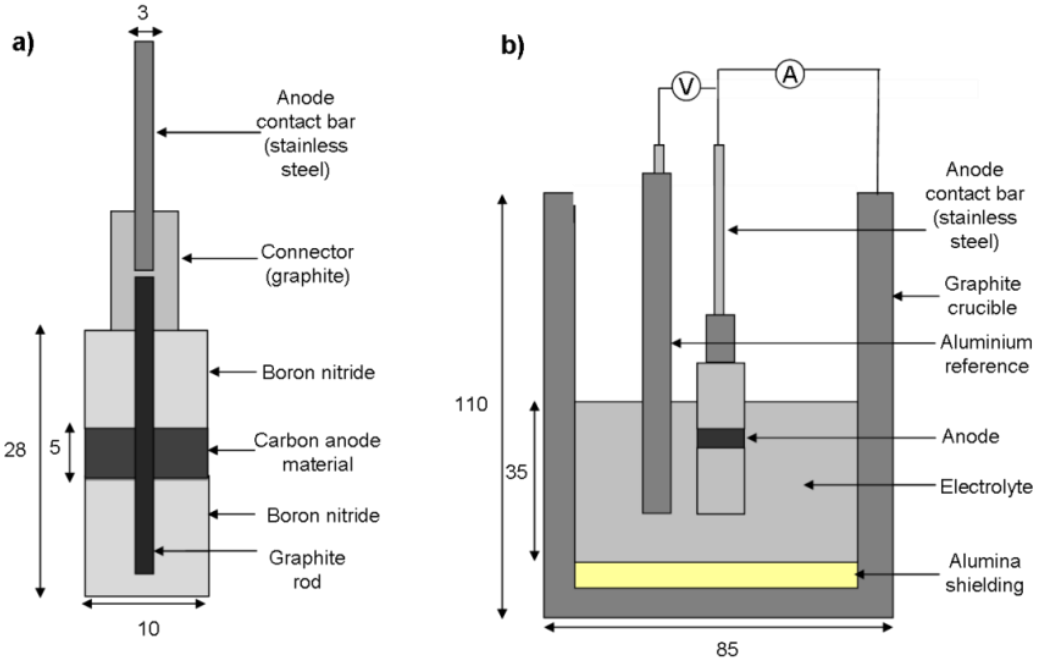
a)
3
Anode contact bar (stainless steel)
Connector (graphite)
Boron nitride
Carbon anode material
Boron nitride
Graphite rod
28
5
10
b)
V
A
Anode contact bar (stainless steel)
Graphite crucible
Aluminium reference
Anode
Electrolyte
Alumina shielding
110
35
85

Figure 2

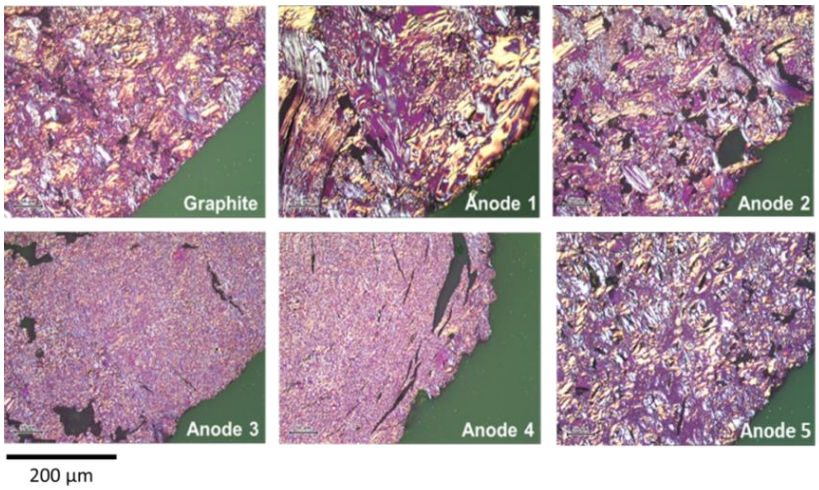

Figure 3

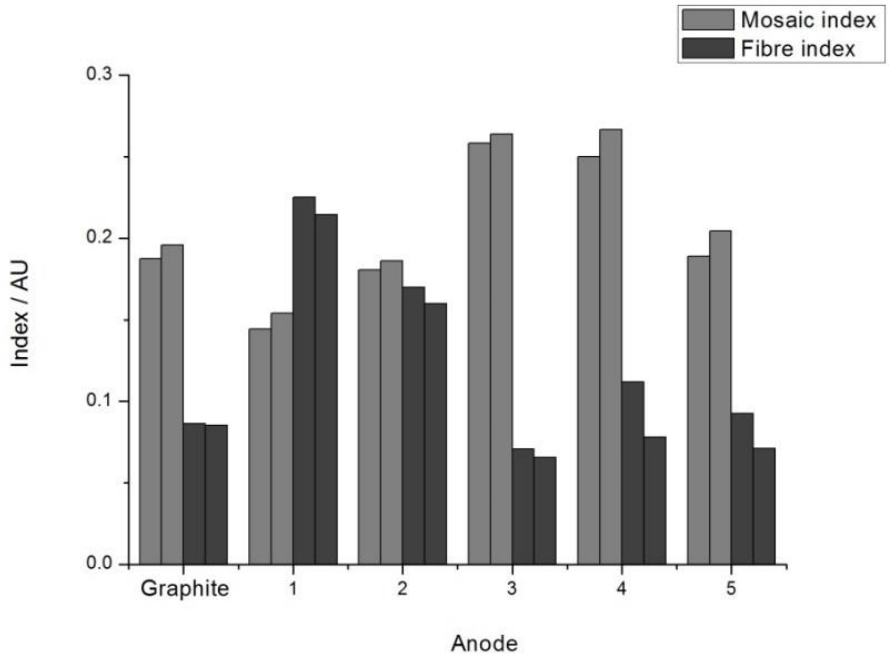
Mosaic index
Fibre index
0.3
0.2
0.1
0.0
Index / AU
Graphite
1
2
3
4
5
Anode

Figure 4

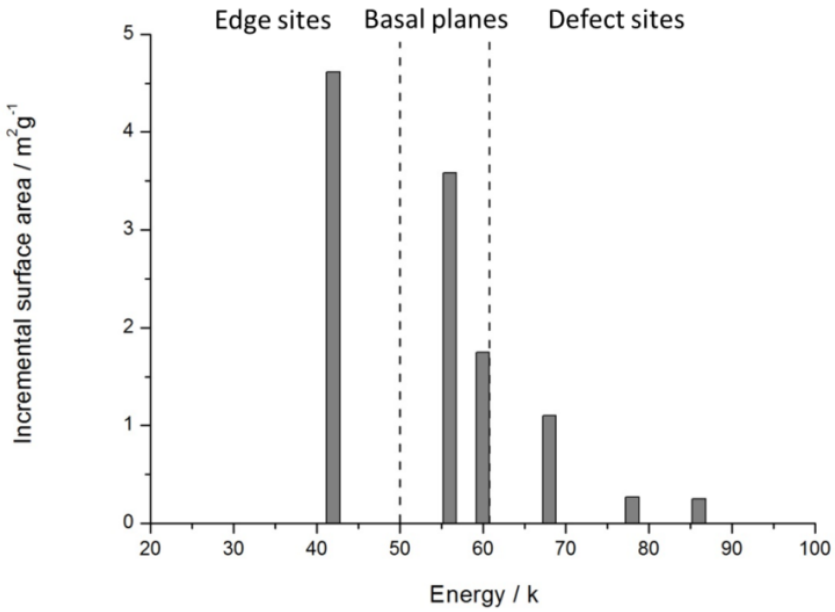
Edge sites
Basal planes
Defect sites
Incremental surface area / m2g-1
Energy / k
0
1
2
3
4
5
20
30
40
50
60
70
80
90
100

Figure 5

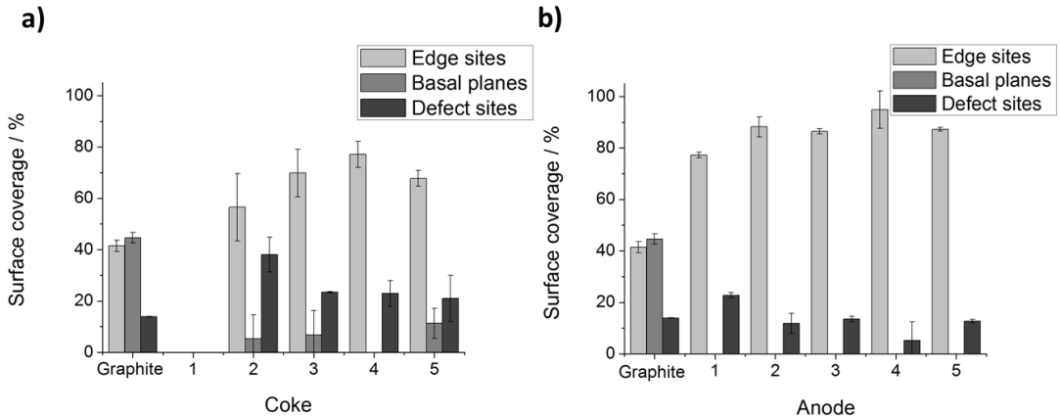
a)
b)
Edge sites
Basal planes
Defect sites
Surface coverage / %
0
20
40
60
80
100
Graphite
1
2
3
4
5
Coke
Anode

Figure 6

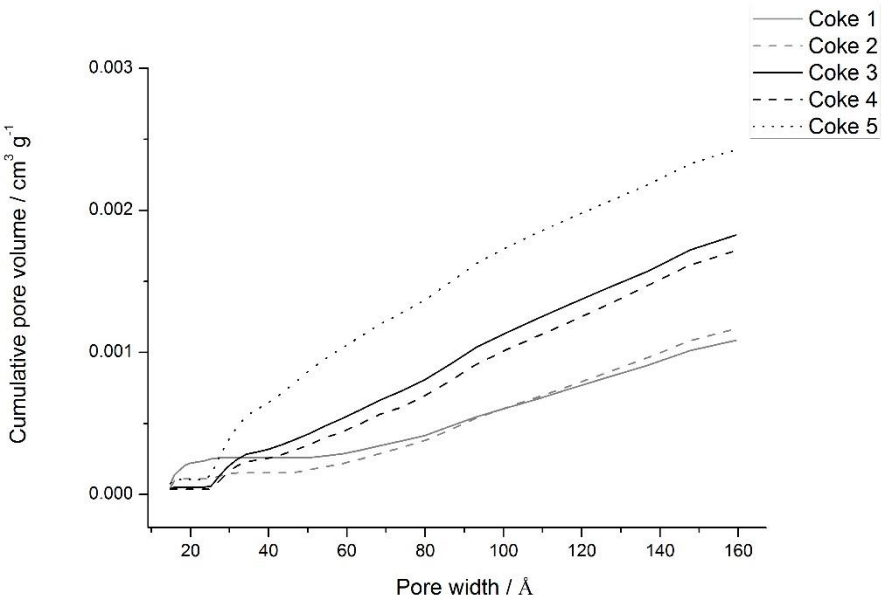
Coke 1
Coke 2
Coke 3
Coke 4
Coke 5
0.003
0.002
0.001
0.000
Cumulative pore volume / cm3 g-1
20
40
60
80
100
120
140
160
Pore width / Å

Figure 7

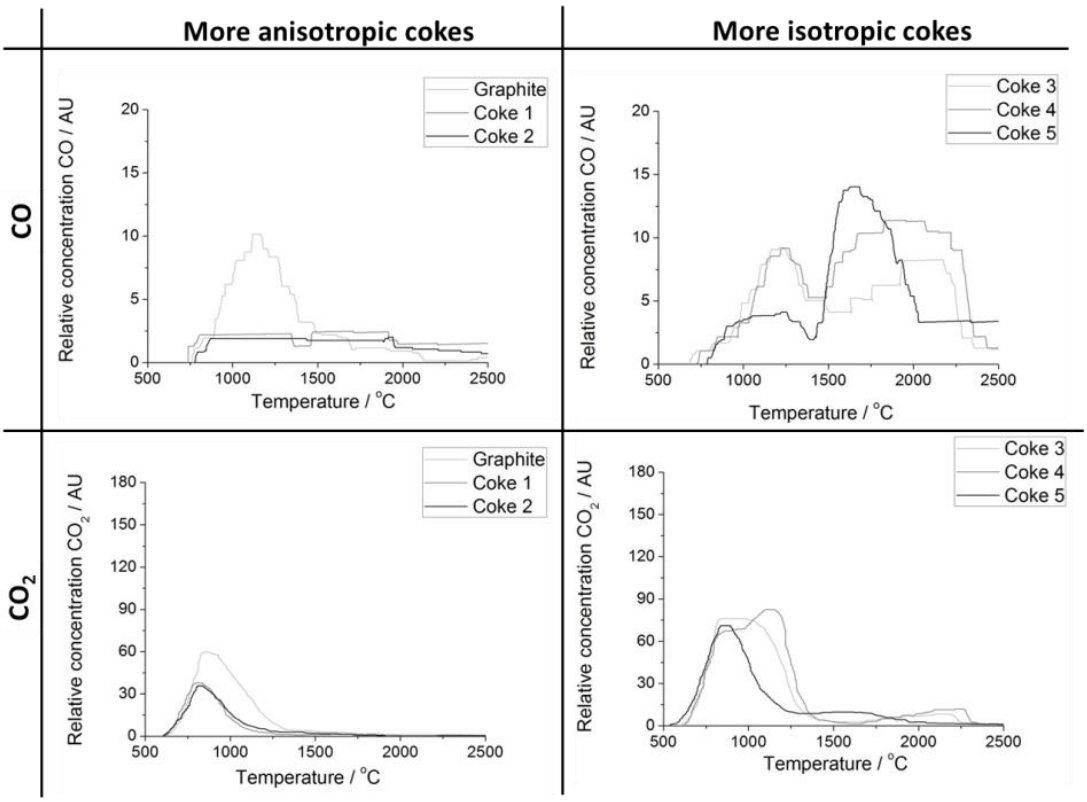
More anisotropic cokes
More isotropic cokes
CO
CO2
Graphite
Coke 1
Coke 2
Coke 3
Coke 4
Coke 5
Relative concentration CO / AU
Relative concentration CO2 / AU
Temperature / °C

Figure 8

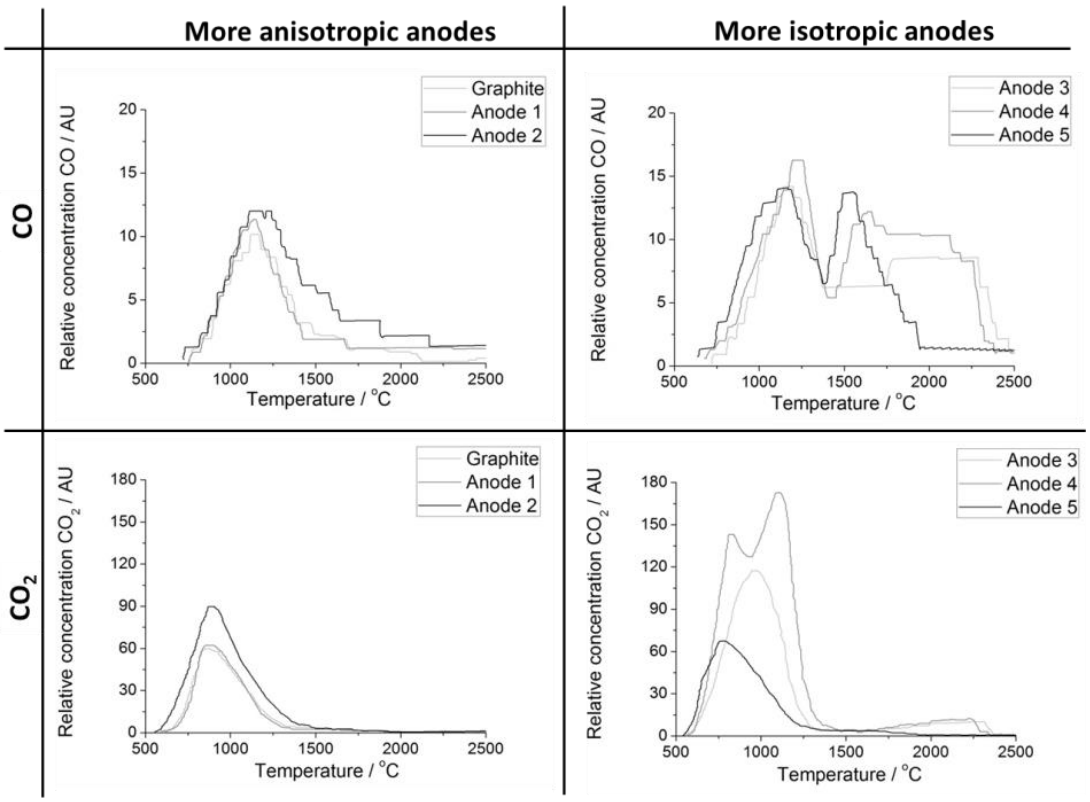
More anisotropic anodes
More isotropic anodes
CO
CO2
Graphite
Anode 1
Anode 2
Anode 3
Anode 4
Anode 5
Relative concentration CO / AU
Relative concentration CO2 / AU
Temperature / °C

Figure 9

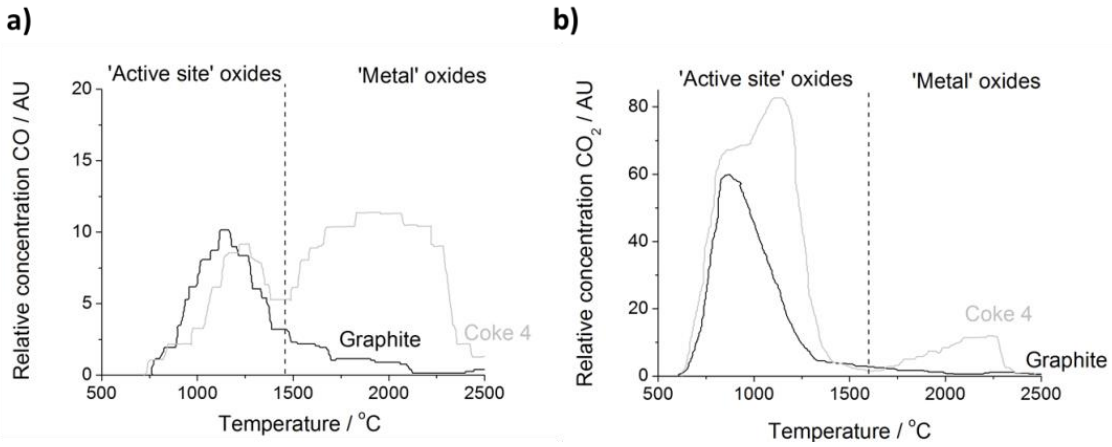
a)
'Active site' oxides
'Metal' oxides
Relative concentration CO / AU
Graphite
Coke 4
Temperature / °C
b)
'Active site' oxides
'Metal' oxides
Relative concentration CO_2 / AU
Coke 4
Graphite
Temperature / °C

Figure 10

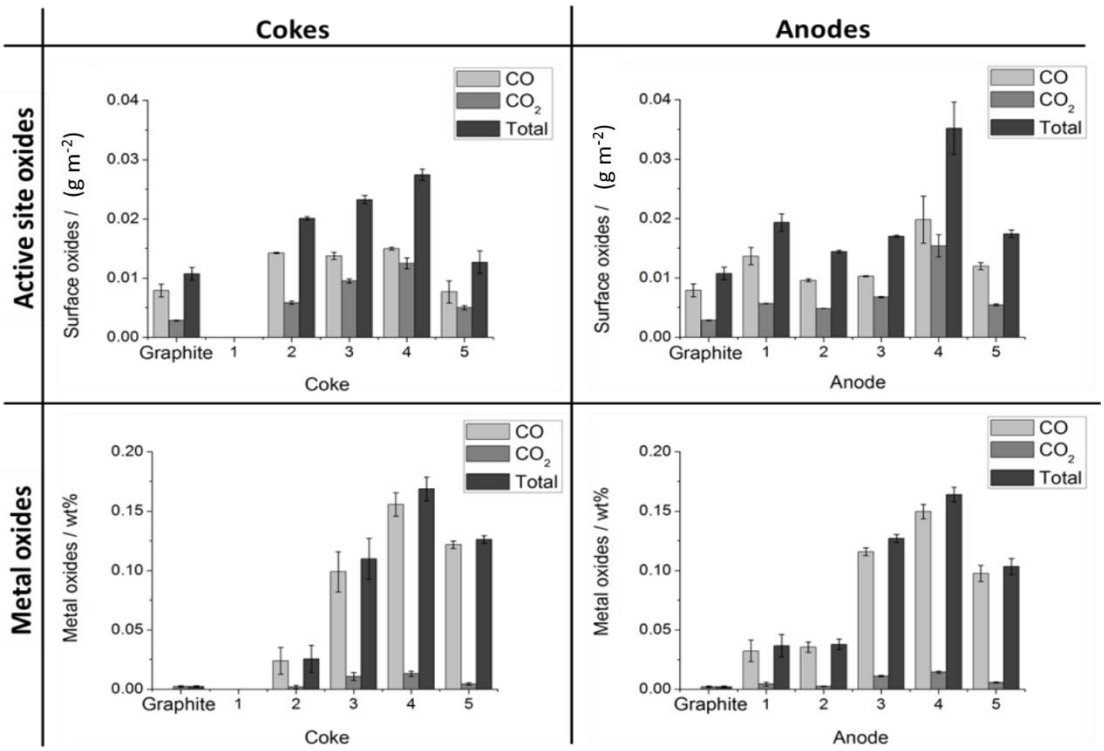
Cokes
Anodes
Active site oxides
Metal oxides
Surface oxides / (g m-2)
Metal oxides / wt%
CO
CO2
Total
Graphite
1
2
3
4
5
Coke
Anode

Figure 11

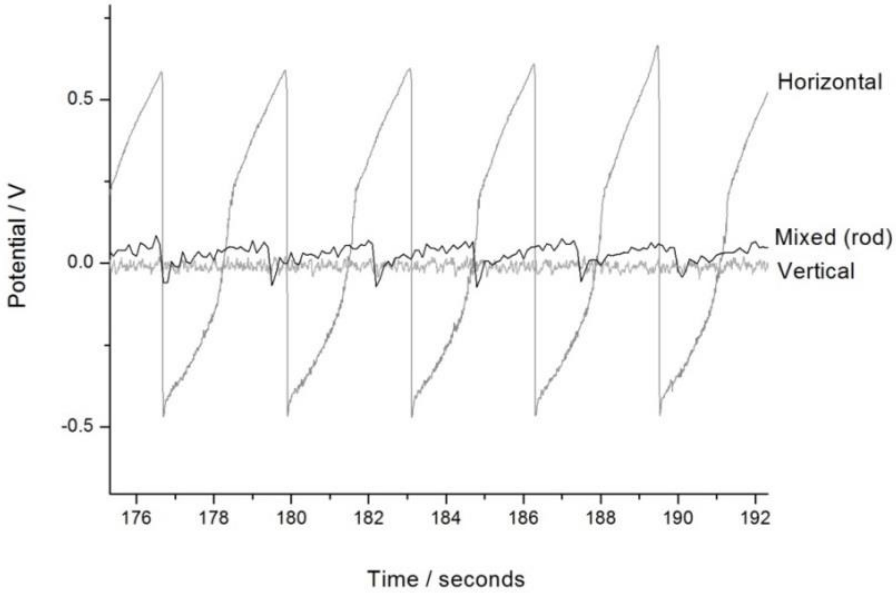
Horizontal
Mixed (rod)
Vertical
Potential / V
0.5
0.0
-0.5
176
178
180
182
184
186
188
190
192
Time / seconds

Figure 12

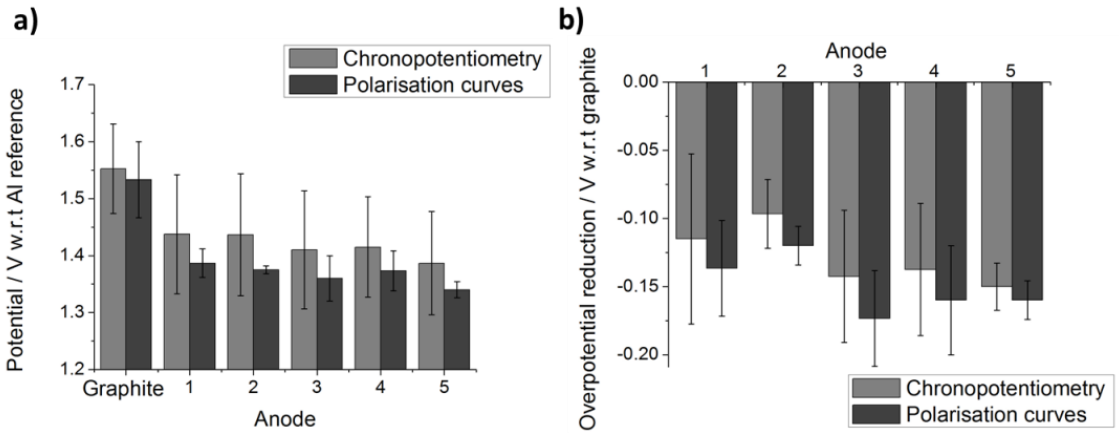
a)
Chronopotentiometry
Polarisation curves
Potential / V w.r.t Al reference
1.7
1.6
1.5
1.4
1.3
1.2
Graphite
1
2
3
4
5
Anode
b)
Anode
1
2
3
4
5
Overpotential reduction / V w.r.t graphite
0.00
-0.05
-0.10
-0.15
-0.20
Chronopotentiometry
Polarisation curves

Figure 13

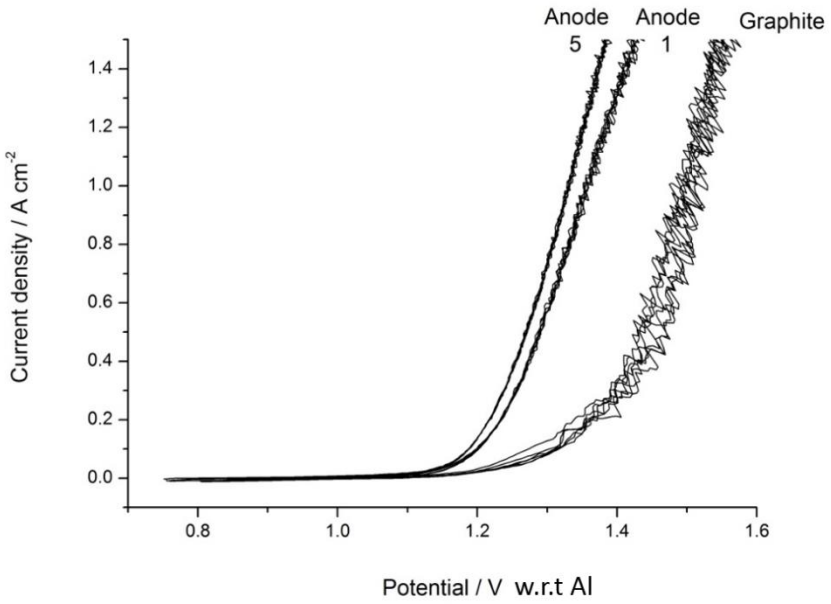
Anode 5
Anode 1
Graphite
Current density / A cm^{-2}
Potential / V w.r.t Al
0.0
0.2
0.4
0.6
0.8
1.0
1.2
1.4
0.8
1.0
1.2
1.4
1.6

Figure 14

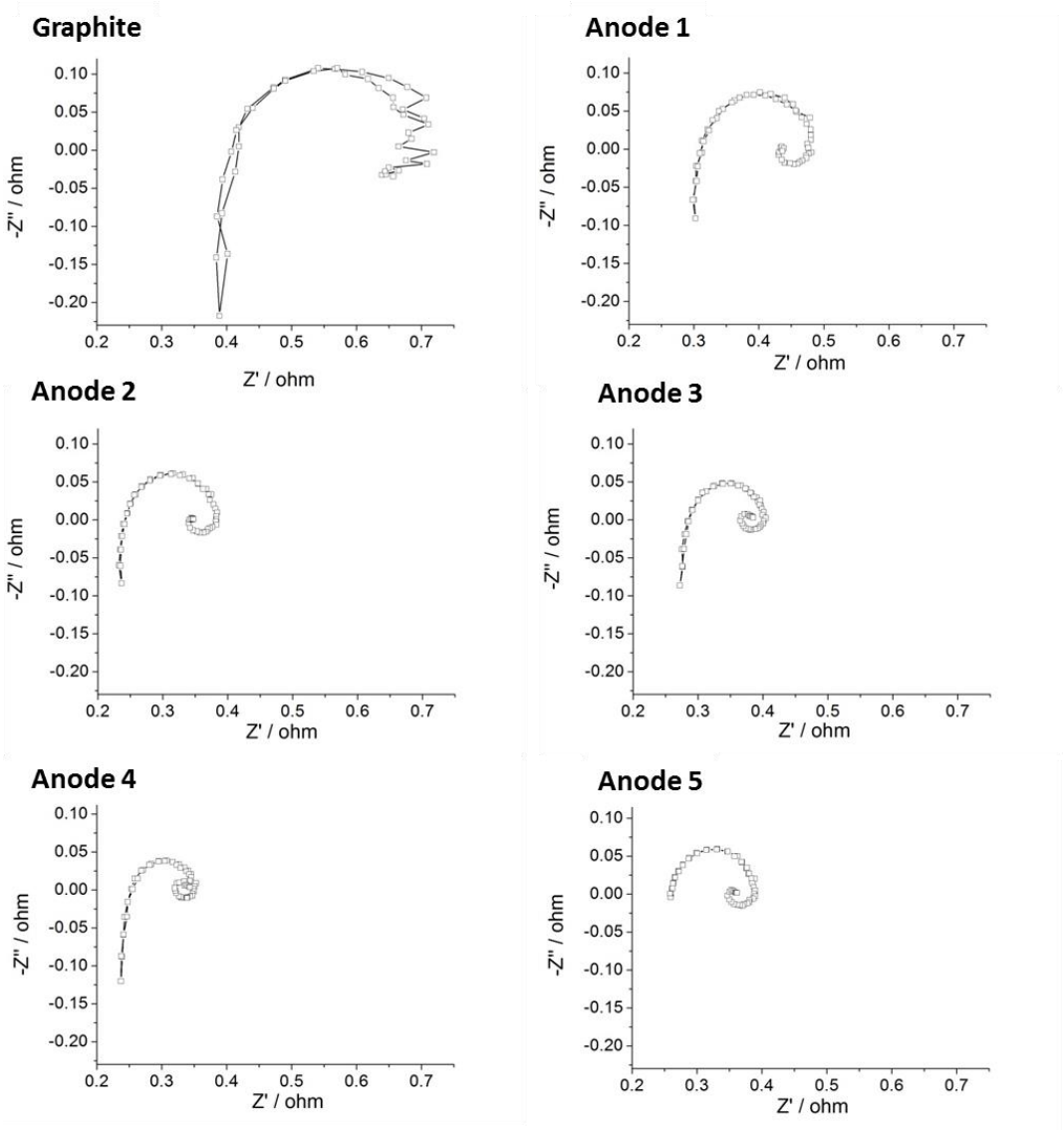
Graphite
Anode 1
Anode 2
Anode 3
Anode 4
Anode 5
-Z'' / ohm
Z' / ohm
0.10
0.05
0.00
-0.05
-0.10
-0.15
-0.20
0.2
0.3
0.4
0.5
0.6
0.7

Figure 15

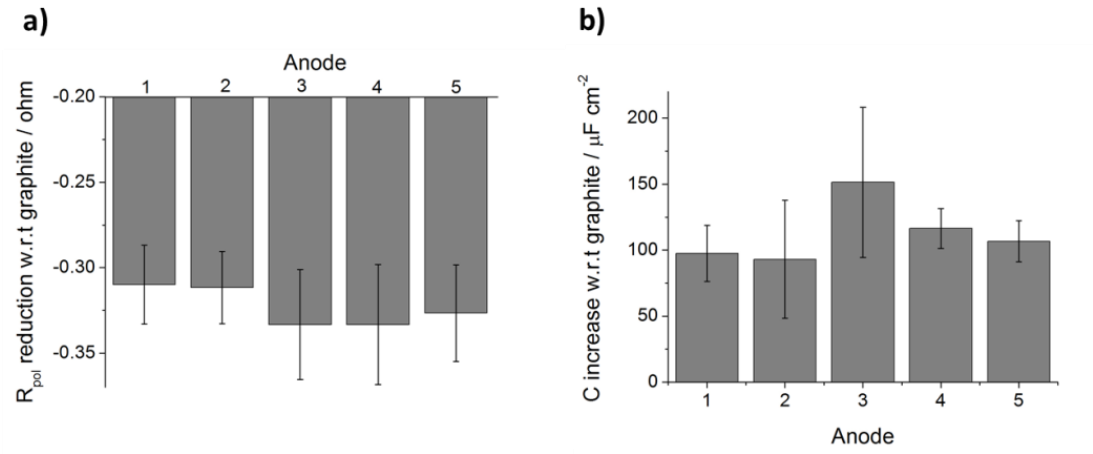
a)
Anode
1
2
3
4
5
-0.20
-0.25
-0.30
-0.35
R_{pol} reduction w.r.t graphite / ohm
b)
C increase w.r.t graphite / μF cm^{-2}
200
150
100
50
0
1
2
3
4
5
Anode

Table and Figure Captions

Table 1. Selected anode properties. Summed metals include Na, Al, Si, Ca, V, Fe and Ni.

Figure 1. a. The anode assembly. b. Location of anode inside graphite crucible.

Figure 2. Optical microscopy images of anodes under polarised light at x250 magnification.

Figure 3. Anode Mosaic and Fibre index. Two parallels are shown for each parameter.

Figure 4. Typical plot of incremental surface area *vs.* energy of graphite and associated definition of edge, basal and defect sites.

Figure 5. Edge site, basal plane and defect site surface coverage (light, medium and dark grey respectively) of a. cokes and b. anodes. Error bars show one standard deviation where n = 2 or 3.

Figure 6. Cumulative pore volume of the coke particles.

Figure 7. Evolved CO and CO_2 from combusted oxides in cokes.

Figure 8. Evolved CO and CO_2 from combusted oxides in anodes.

Figure 9. Evolution of a. CO and b. CO_2 from ultrapure graphite and Coke 4, the coke used to make Anode 4. Integration cut-off for calculation of surface (edge site) oxides and metal oxides is shown.

Figure 10. Surface oxygen, normalised with respect to BET surface area and metal oxide concentrations of graphite and the cokes/anodes. Individual contributions from evolved CO (light grey) and CO_2 (medium grey) are shown along with total contributions (dark grey). Error bars show one standard deviation where n = 3.

Figure 11. Potential of graphite anodes (V w.r.t Al) with varying geometry at 1 A cm^{-2}, normalised around zero to show potential oscillation.

Figure 12. a. Anode potential at 1 A cm^{-2} (V w.r.t Al) and b. Reduction in overpotential of the materials tested at 1 A cm^{-2}, quoted with respect to graphite for each set of data. Error bars show one standard deviation where n = 4 for chronopotentiometry and n = 3 for polarisation curves.

Figure 13. IR corrected polarisation curves of graphite and anodes 1 and 5. Three consecutive polarisation curves are shown for each material (V w.r.t Al).

Figure 14. Unfitted Nyquist spectra from EIS measurements at an applied voltage of 1.4 V w.r.t Al.

Figure 15. a. Anode polarisation resistance, R_{pol} and b. Capacitance, C, at an applied voltage of 1.4 V w.r.t Al. Averages and standard deviation are calculated from three anode parallels (n = 3) and are quoted w.r.t graphite.